Smart Structures and Systems, *Vol. 26, No. 5* (*2020*) *619-629*
DOI: https://doi.org/10.12989/sss.2020.26.5.619

Mitigation of wind-induced responses of cylinder solar tower by a tiny eddy current tuned mass damper based on elastic wind tunnel tests

Min Liu[a], Shouying Li[*] and Zhengqing Chen[b]

Key Laboratory for Wind and Bridge Engineering of Hunan Province, College of Civil Engineering, Hunan University, Changsha 410082, China

(*Received December 2, 2019, Revised May 16, 2020, Accepted July 29, 2020*)

Abstract. Solar towers, which often has a large aspect ratio and low fundamental natural frequency, were extremely prone to large amplitude of wind-induced vibrations, especially Vortex-Induced Vibration (VIV). A tiny Tuned Mass Damper (TMD) with conveniently adjustable eddy current damping was specially designed and manufactured for elastic wind tunnel tests of a solar tower. A series of numerical simulations by using the COMSOL software were conducted to determine three key parameters, including the thickness of the back iron plate and the conductive plate (T_b and T_c), the distance between the magnet and the conductive plate (T_d). Based on the results of numerical simulations, a tiny TMD was manufactured and its structural parameters were experimentally identified. The optimized values of the tiny TMD can be conveniently realized. The tiny TMD was installed at the top of the elastic test model of a 243-meter-high solar tower, and a series of wind tunnel tests were carried out to examine the effectiveness of the TMD in suppressing wind-induced responses of the test model. The results showed that the wind-induced responses could be obviously reduced by the TMD, especially in the cross-wind direction. The cross-wind RMS and peak responses at the critical wind velocity can be reduced by about 86% and 75%, respectively. However, the maximum reduction of the responses at the design wind velocity is about 45%, obviously less than that at the critical wind velocity.

Keywords: solar tower; tuned mass damper; eddy current damping; vortex-induced vibration; wind tunnel tests

1. Introduction

Solar towers were built all over the world in recent years (González-Roubaud *et al*. 2017, Tahri *et al*. 2015). This kind of structures often has large aspect ratio, low fundamental natural frequency and small structural damping, which indicates that they are extremely prone to wind-induced vibrations, especially the Vortex-Induced Vibration (VIV) in the across-wind direction. Li *et al*. (2018) and Liu *et al*. (2019) carried out a series of elastic wind tunnel tests to study the wind-induced responses of the Noor III solar tower. This solar tower has a height of 243 m, an aspect ratio of about 12 and a fundamental natural frequency of 0.28 Hz. Large amplitude VIV response of the Noor III solar tower was observed in the across-wind direction under the structural damping ratio of 0.7%, and it seems that the measured base forces in the wind tunnel tests were obviously greater than the values stipulated in American Code ACI 307-08. This indicates that some countermeasures should be adopted to reduce the across-wind VIV responses of solar towers.

Many types of aerodynamic countermeasures, such as tapered and corner modified, were often adopted to reduce the wind-induced VIV responses of high-rise buildings by changing their configurations (Isyumov *et al*. 1989, Quan and Gu 2005, Tanaka *et al*. 2012, Bandi *et al*. 2013, Kim *et al*. 2014, 2015, Tamura *et al*. 2017). For the chimneys which usually have circular cross sections like solar towers, the wind-induced VIV responses can also be effectively reduced by installing helical wires on their surface (Zdravkovich 1981), and this countermeasure was even suggested in some codes and standards (CICIND 1999). Unfortunately, these effective aerodynamic countermeasures could not be used on solar towers because that most of the outer surface of solar towers should keep smooth to realize the function of absorbing solar energy.

Another effective countermeasure to mitigate the wind-induced responses of high-rise structures is to install Tuned Mass Dampers (TMDs). The TMD concept was firstly invented by Frahm in 1909, and the optimized structural parameters of the TMD related to an undamped structure were theoretically deduced by Den Hartog (1956). Up to now, the TMD system was successfully adopted to mitigate the wind-induced responses on a lot of high-rise structures all over the world. Two pendulum-type TMDs, one at the top of the turret and the other at the intermediate platform, were installed on the Sydney tower in Australia, and noticeable reductions of the wind-induced responses were observed (Vickery and Davenport 1971, Kwok 1983). On the 553-meter-high CN tower in Toronto, two TMDs were attached to the antenna mast to reduce the vibrations of the second and fourth modes (Sacks and Swallow 1993). On the

*Corresponding author, Professor,
E-mail: shyli@hnu.edu.cn
[a] Student, E-mail: 464933874@qq.com
[b] Professor, E-mail: zqchen@hnu.edu.cn

ISSN: 1738-1584 (Print), 1738-1991 (Online)

Chiba port tower in Japan, a slide platform-type TMD was installed to reduce the vibrations caused by both strong winds and earthquakes, and the results showed that the wind-induced responses of this tower could be reduced by nearly 50% in all wind directions (Kitamura *et al*. 1988, Ohtake *et al*. 1992). Brownjohn *et al*. (2010) found that TMD system was effective in suppressing the wind-induced response of a 183-meter-high reinforced concrete chimney. There are also many structures recently installed with TMDs such as the Citicorp building in New York city, the Aspire tower in Doha, Qatar and the 634-meter-high Tokyo skytree in Tokyo, Japan (Mariantonieta and Hojjat 2013). Two famous examples for the TMD applications in China is the Taipei 101 tower and the 600-meter-high Canton tower in Guangzhou (Tuan and Shang 2014, Xu *et al*. 2014). Besides the high-rise structures, there were also some successful applications of TMD system on large span bridges, for instance the Akashi Kaikyo bridge in Japan (Koshimura *et al*. 1994).

TMD system is an energy absorber in nature, and the absorbed energy should be dissipated by dampers incorporated in the TMD system. At present, the most widely used damper in TMD system is fluid viscous damper (Mcnamara and Taylor 2003, Narkhede and Sinha 2014). This type of dampers has some shortcomings in the leak of working fluid because of the easy ageing of the sealing rubber. Moreover, this type of dampers does not work under low level of main structure response because there exists a large initial friction force in the damper. One recently developed damping technology, called Pounding Tuned Mass Damper (PTMD) which can work in a confined space with a small mass ratio, seems to be able to overcome some shortcomings of the fluid viscous damper (Wang *et al*. 2018a, b, Duan *et al*. 2020). However, there is a disadvantage for PTMD that a large acceleration pulse would be produced in controlled structure, and this will be harmful to human comfort control. Another promising damping technology is eddy current damping, which was usually adopted to reduce machine vibration in mechanical field from several decades ago (Gunter *et al*. 1983, Cunningham 1986, Sakamoto *et al*. 1997, Ebrahimi *et al*. 2009). Kienholz *et al*. (1994) designed an eddy current TMD to successfully suppress the vibration of a solar panel. Huang *et al*. (2018) proposed a new type of eddy current damper and found that the use of a back iron increases the damping coefficient by a factor of up to 5. In recent years, the eddy current damping begins to be applied on the civil engineering structures. For example, a pendulum-type TMD with eddy current damping was installed at the height of 578.2 m of the 632-meter-high Shanghai center tower in China to reduce its wind-induced responses (Lu and Chen 2011, Lu *et al*. 2017). Over 10 eddy current TMDs were installed on the Mianyan first bridge in China to reduce the human-induced vibrations (Wen *et al*. 2016). Some researchers found that the eddy current damping is suitable to accurately provide the damping in the model tests. Larose *et al*. (1995) proposed a cantilever-type TMD system with eddy current damping to mitigate the vortex-induced vibration of an elastic bridge model with a geometric scale of 1:125 in wind tunnel tests. Kwak *et al*. (2003) and Bae *et al*. (2005) both designed an eddy current damper to successfully reduce the vibration of a cantilever beam test model. Lou *et al*. (2019) carried out parametric study of a cantilever-type eddy current damper for a lattice tower test model and applied to control bidirectional wind-induced vibration of the tower model. On the model test, it is difficult to conveniently adjust the parameters of the TMD because of the small size.

In this paper, a tiny eddy current TMD with mass ratio of 1%, that is the mass of the TMD is only 5×10^{-3} kg, was carefully designed and manufactured, and was used in the wind tunnel tests for the model of a 243-meter-high solar tower to validate the effectiveness of the TMD on mitigating its wind-induced responses. The damping coefficient of the TMD system was investigated by both numerical simulations and experimental measurements. This tiny TMD system was installed at the top of the elastic test model, and a series of wind tunnel tests were carried out to obtain the wind-induced responses of the solar tower with and without the TMD system. The effectiveness of the TMD system is carefully examined.

2. Description of the elastic test model

A full-elastic test model for a 243-meter-high solar tower was designed and manufactured to realize the structural damping ratio as low as 0.3% by Li *et al*. (2018). The Froude number and the Reynolds number were not taken into account in the design of the elastic test model. The length scale of the test model is 1/200, and the velocity scale of the test model, which is determined through the first natural frequency of the test model, is 1/5.97. Structural analyses by using the ANSYS software show that the first natural frequency and the generalized mass of the first mode of this prototype solar tower are 0.28 Hz and 4.27×10^6 kg, respectively. More detailed information of the prototype tower and its elastic test model could be found in Li *et al*. (2018).

Wind-induced responses of this solar tower were investigated by means of wind tunnel tests (Li *et al*. 2018), and obvious VIV response was found within the wind velocity range of U_{10} = 21.5~28.4 m/s (at the height of 10 m) for the structural damping ratio of 0.7%. This critical wind velocity is far less than the design velocity of the solar tower. Moreover, the base forces measured from the wind tunnel tests are far higher than the values determined by the code of ACI 307-08, which is adopted to the structural design of this solar tower.

3. Design and manufacture of the Tiny TMD

3.1 Determination of the structural parameters for the Tiny TMD

As we know, the mass ratio μ, which is the mass of TMD to that of the main structure, has important effect on the effectiveness of the TMD system. The effectiveness of the TMD system can be obviously enhanced by increasing

the mass ratio. However, the expenditure of the TMD system increases with the increase of the mass ratio. Furthermore, a large mass ratio might have adverse effect on the earthquake responses of the main structure. So, it is important to determine a reasonable value of the mass ratio of the TMD system. According to the previous studies, the wind-induced vibration of high-rise structures could be obviously mitigated by the mass ratio in the order of 1% to 2% of the modal mass for TMD systems (Facioni *et al*. 1993, Ohtake *et al*. 1992, Kawamura *et al*. 1993). Li *et al*. (2018) found that the wind-induced response of the solar tower is dominantly come from the first mode. This indicates that it is rational to determine the structural parameters of the TMD system based on the first mode of the solar tower. For the prototype TMD of this 243-meter-high solar tower, 1% of mass ratio corresponding to the first mode is adopted in this study. The generalized mass of the first mode of the solar tower is 4.27×10^6 kg, which means that the mass of the prototype TMD is 4.27×10^4 kg. In consideration of the length scale of the elastic test model of the solar tower, 1/200, the mass of the tiny TMD for the test model is about 5×10^{-3} kg.

Since the structural damping of the studied solar tower is very small, the optimized frequency ratio α_{opt}, which is the natural frequency of the TMD system to that of the target mode of the solar tower, could be determined from the mass ratio μ as follows (Den Hartog 1956)

$$\alpha_{opt} = \frac{1}{1+\mu} \tag{1}$$

According to Eq. (1), α_{opt} is about 0.99 for 1% of the mass ratio μ, which indicates that the natural frequency of the prototype TMD system should be 0.277 Hz in light of the first natural frequency of the solar tower (0.28 Hz). The frequency scale of the test model of the solar tower is 1/33.5, and the target optimized natural frequency of the tiny TMD for the test model is about 9.28 Hz.

Another important structural parameter of the TMD system is the optimized damping ratio ξ_{opt}, which could be determined by Den Hartog (1956)

$$\xi_{opt} = \sqrt{\frac{3\mu}{8(1+\mu)}} \tag{2}$$

Therefore, the target optimized damping ratio of the TMD system is about 6% according to 1% of the mass ratio. It should be noted that the optimized damping ratios for the prototype and tiny TMD systems are both 6% because it is a non-dimensional parameter.

3.2 Realization of the structural stiffness for the Tiny TMD

The prototype TMD system on the high-rise structures is often designed as a pendulum. The oscillation frequency of a pendulum-type TMD can be directly determined by

$$f = \frac{1}{2\pi}\sqrt{\frac{g}{l}} \tag{3}$$

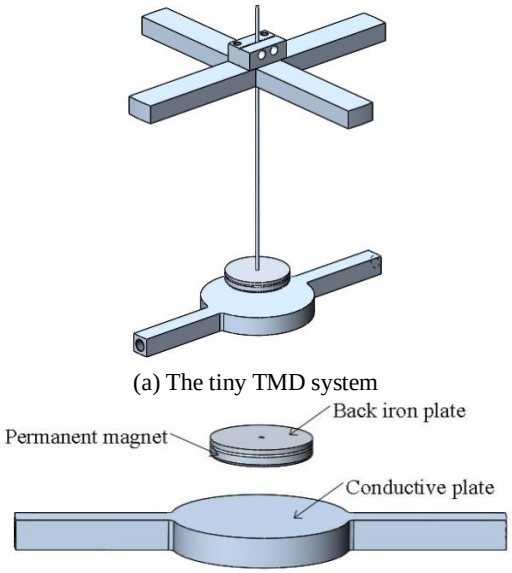

(a) The tiny TMD system

(b) The eddy current damper

Fig. 1 The sketch map of the tiny TMD system

where, l is the pendulum length; g is the acceleration of gravity, here g = 9.8 m/s^2. In the present study, the pendulum length of the prototype TMD system for the solar tower is approximately 3 meter according to the natural frequency of 0.277 Hz. This indicates that the pendulum length of the tiny TMD system for the test model is only about 15 mm in light of 1/200 of the length scale for the elastic test model. However, the natural frequency of a pendulum with a length of 15 millimeter is about 4.07 Hz, which is not corresponding to the optimized natural frequency of the tiny TMD for the test model (9.28 Hz). This is because the Froude number is not taken into account in the design of the elastic test model. At this moment the velocity scale is not equal to the square root of the length scale. Therefore, the pendulum length of the tiny TMD system should be determined from Eq. (3) by using the optimized natural frequency of the tiny TMD (9.28 Hz), which indicates that the pendulum length of the tiny TMD is about 3 millimeter. It is very difficult to achieve a pendulum with a pendulum length as short as 3 mm. In this study, a cantilever beam is adopted to provide the stiffness of the tiny TMD for the test model, and the target natural frequency of the tiny TMD can be conveniently achieved by adjusting the length, the material and the cross section of this cantilever beam. The top of the elastic test model, as described in Li *et al*. (2018), is a cup-shaped coat without core beam. The room within the top coat, which has a height of 215 mm and a diameter of 150 mm, is reserved to accommodate the tiny TMD (Li *et al*. 2018). The cross section and the material of the cantilever beam should be carefully determined to ensure that the tiny TMD system could be accommodated in the reserved room. A steel bar, which has a circular cross section with a diameter of 1 mm, is designed to realize the stiffness of the tiny TMD, as shown in Fig. 1(a). According to the mass and natural frequency of the tiny TMD (5×10^{-3} kg and 9.28 Hz), the length of the steel bar is approximately 100 mm.

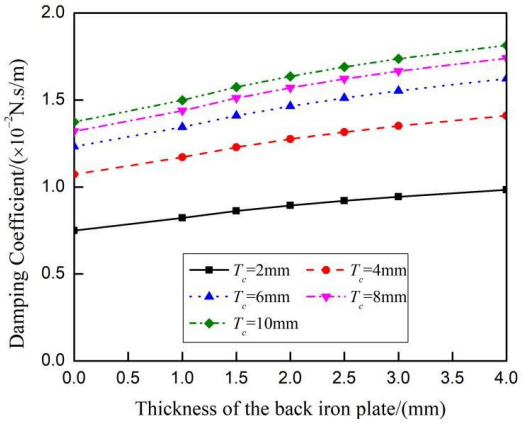

Fig. 2 The effects of the thickness of the back iron plate on the eddy current damping coefficient (T_d = 5 mm)

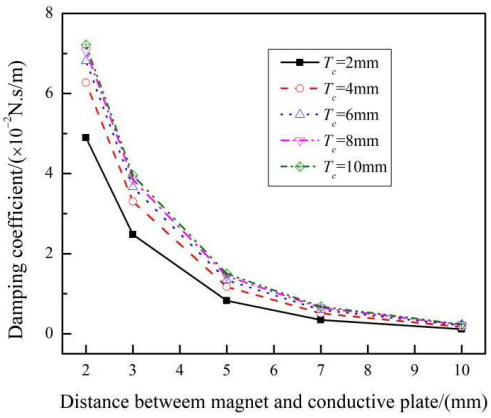

Fig. 4 The effects of the distance between magnet and conductive plate on the eddy current damping coefficient (T_b = 1 mm)

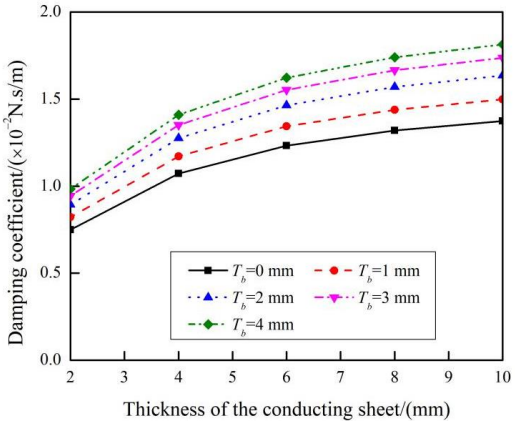

Fig. 3 The effects of the thickness of the conductive plate on the eddy current damping coefficient (T_d = 5 mm)

3.3 Realization of the structural damping for the Tiny TMD

The damping of the tiny TMD is provided by an eddy current damper which consists of a permanent magnet and a conductive plate, as shown in Fig. 1. The relative motion between the magnet and the conductive plate produces eddy currents in the conductive plate, and an electromagnetic force could be generated between the magnet and the conductive plate. This electromagnetic force is linearly related with the relative velocity and dissipates the kinetic energy of the TMD into thermal energy.

The permanent magnet adopted is the NdFeB magnet, which has a ring shape with a thickness of 2 mm, an outer diameter of 20 mm and a mass of 2.5 × 10^{-3} kg. In order to enhance the efficiency of the permanent magnet, a back iron plate with a diameter of 20 mm is adopted, and the steel bar is connected with the back iron plate at its center point, as shown in Fig. 1. The material of the conductive plate is aluminum, which has a lower density and moderate conductivity compared with copper and zinc. This ensures that the total mass of the test model could be completely satisfied as well as linear damping properties for the tiny TMD system. The diameter of the conductive plate is 35 mm, which is 1.75 times of the outer diameter of the magnet. This ensures that the conductive plate could incise the magnetic field completely. Two aluminum bar are manufactured together with the conductive plate to connect the conductive plate with the top coat of the test model through two M3 screw spikes.

Three parameters, including the thickness of the back iron plate and conductive plate (T_b and T_c), the distance between the magnet and the conductive plate (T_d), should be determined to realize the target damping ratio of the tiny TMD system (6%). In order to determine the reasonable values of the three aforementioned parameters, the software COMSOL was adopted to conduct a series of numerical simulations in which the permanent magnet is regarded as a linear magnetization model. and the effects of the parameters on the eddy current damping coefficient are carefully investigated.

Fig. 2 presents the variations of the eddy current damping coefficient of the tiny damper with the thickness of the back iron plate under different thickness of the conductive plate (T_c = 2, 4, 6, 8, 10 mm) obtained from the numerical simulations. It should be noted that the distance between the permanent magnet and the conductive plate is 5 mm. From Fig. 2, it could be found that the eddy current damping coefficient slightly increases with the thickness of the back iron plate. According to the mass and natural frequency of the tiny TMD (5 × 10^{-3} kg and 9.28 Hz), the target damping coefficient for damping ratio of 6% should be 0.035 N·s/m. It appears that the damping coefficient is lower than 0.02 N·s/m even if the thickness of the conductive plate and the back iron plate should respectively be 10 mm and 4 mm. However, the total mass of the tiny TMD system will be far greater than 5 × 10^{-3} kg if the thickness of the back iron plate is 4 mm. Therefore, it seems that the distance between the magnet and the conductive plate should be adjusted to reduce the thickness of the back iron plate.

Fig. 3 presents the variations of the eddy current damping coefficient of the tiny damper with the thickness of the conductive plate under different thickness of the back iron plate (T_b = 0, 1, 2, 3, 4 mm) obtained from the

Fig. 5 The tiny TMD system used to experimentally identify its structural parameters

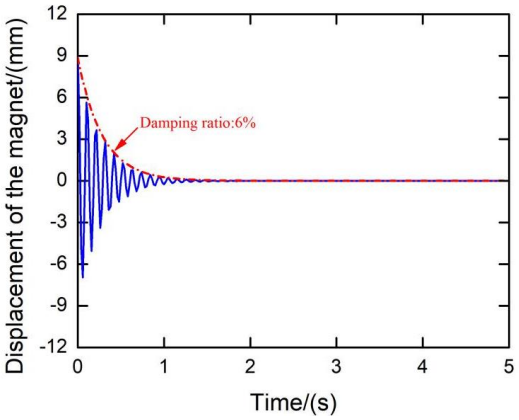

Fig. 6 A typical time histories of the displacement of the free vibration of the tiny TMD for damping ratio of 6%

numerical simulations. It should be noted that the distance between the permanent magnet and the conductive plate is 5 mm. From Fig. 3, it could be found that the eddy current damping coefficient obviously increases with the increasing of the thickness of the conductive plate, especially within the thickness range of 2~4 mm.

Fig. 4 shows the variations of the eddy current damping coefficient of the tiny damper with the distance between the magnet and the conductive plate under different thickness of the conductive plate (T_c = 2, 4, 6, 8, 10 mm). The thickness of the back iron plate is 1mm in Fig. 4. It could be found from Fig. 4 that the damping coefficient of the tiny damper sharply decreased with the increasing of the distance between the magnet and the conductive plate. It seems the target damping coefficient, 0.035 N·s/m, will be well satisfied if T_b = 1 mm, T_c = 6 mm and T_d = 3 mm.

Based on the results of numerical simulations given in Figs. 2-4, The thicknesses of the back iron plate and the conductive plate are respectively chosen to be 1 mm and 6 mm, that is T_b = 1 mm and T_c = 6 mm. At this time, the target damping coefficient of 0.035 N·s/m, which is corresponding to the damping ratio of 6%, can be achieved with the distance of the magnet and the conductive plate of approximately 3 mm. It should be noted that the distance between the magnet and the conductive plate could be conveniently adjusted through shifting the conductive plate up and down.

Table 1 Main structural parameters used in the tiny TMD

Structural parameters	Values
Mass	5×10^{-3} kg
Length of the steel bar	95 mm
Thickness of the back iron plate	1 mm
Thickness of the conductive plate	6 mm
Distance between the magnet and the conductive plate	2.5 mm
Damping ratio	6%

(a) The elastic test model

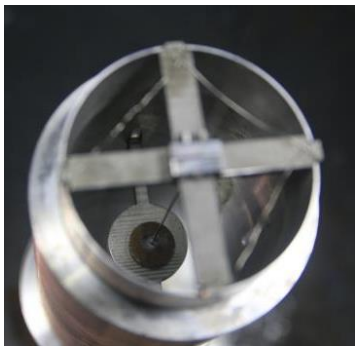

(b) The tiny TMD at the top

Fig. 7 Photos of the test model with the tiny TMD installed in the wind tunnel

3.4 Identification of the structural parameters of the Tiny TMD

The proposed tiny TMD system, which is composed of the permanent magnet, the back iron plate, the steel bar and the conductive plate, was installed on a test frame, as shown in Fig. 5. The natural frequency of the tiny TMD system could be conveniently adjusted by changing the length of the steel bar, and the desired damping coefficient could be adjusted by changing the distance between the permanent magnet and the conductive plate. The natural frequency and the damping ratio of the tiny TMD system could be identified from the free vibration responses by frequency domain approach and logarithmic decrement method, respectively.

Based on the experimental identification, the target natural frequency of the tiny TMD, 9.28 Hz, could be

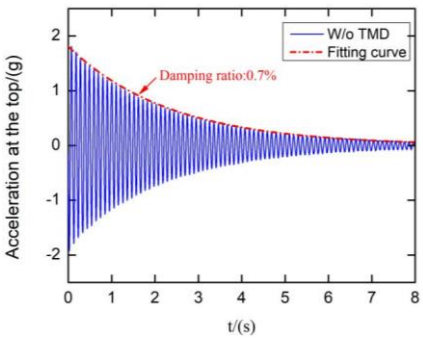

(a) Without TMD

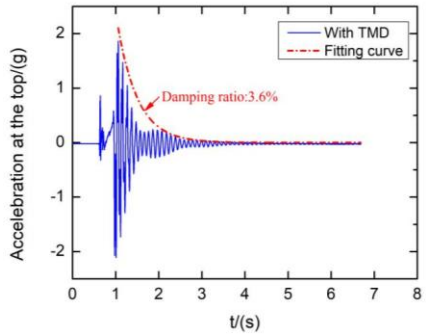

(b) With TMD

Fig. 8 Time histories of the free vibration acceleration at the top of the test model with and without TMD

achieved if the length of the steel bar is 95 mm. Fig. 6 presents a typical time histories of the displacement of the free vibration of the tiny TMD, which is corresponding to the target damping ratio, 6%. Under the circumstances, the distance between the magnet and the conductive plate is 2.5 mm, which is slightly smaller than the value obtained from the numerical simulation, 3.0 mm.

Based on the numerical simulation and experimental identification, the main structural parameters used in the tiny TMD are listed in Table 1.

4. Outline of wind tunnel tests

The tiny TMD designed in Section 3 was installed on the top of the elastic test model of the solar tower introduced by Li *et al*. (2018), as shown in Fig. 7(b). A series of wind tunnel tests were carried out on the elastic test model to validate the effectiveness of the eddy current TMD on mitigating the wind-induced vibration of the solar tower, especially the vortex-induced vibration in the across-wind direction. Wind tunnel tests were carried out in the closed-circuit test section of the HD-2 Boundary Layer Wind Tunnel (HD-2BLWT) of Hunan university, Changsha, China. This test section has a size of 3.0 m in width by 2.5 m in height by 17.0 m in length, and its maximum wind velocity is 58 m/s. The category type C stipulated in the ASCE/SEI 7-10 is used in this wind tunnel tests, which is the same as Li *et al*. (2018). The reference height, at which a Cobra probe is installed to measure the wind velocity in the wind tunnel, is 1.0 m over the ground. The range of wind velocity at the reference height in the wind tunnel tests

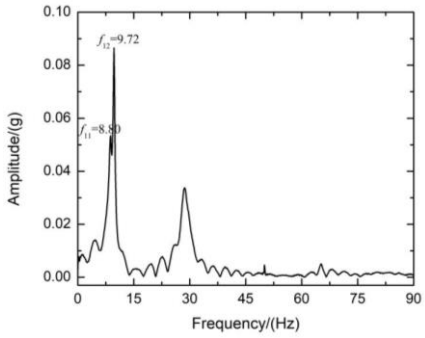

Fig. 9 Power spectrum densities of the free vibration acceleration at the top of the test model with the TMD

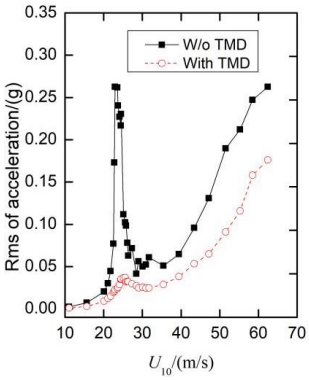

(a) Acceleration at the top

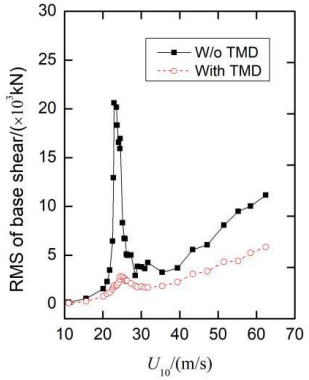

(b) Base shear

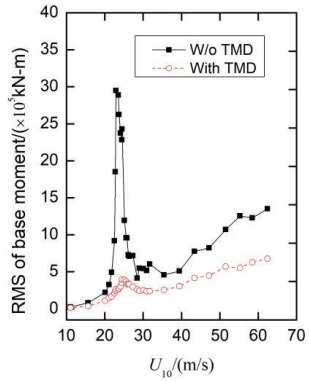

(c) Base moment

Fig. 10 Comparisons of the across-wind RMS responses of the solar tower with and without the TMD system

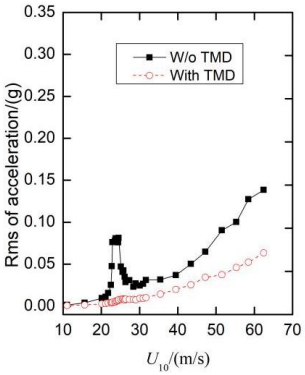

(a) Acceleration at the top

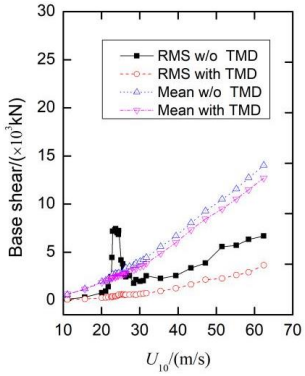

(b) Base shear

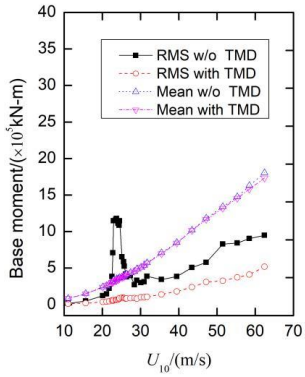

(c) Base moment

Fig. 11 Comparisons of the along-wind responses of the solar tower with and without the TMD system

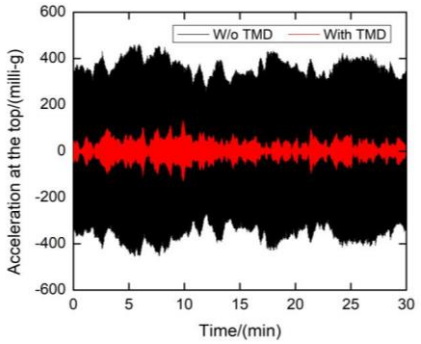

(a) Cross-wind

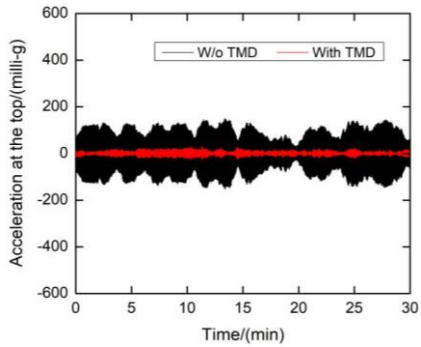

(b) Along-wind

Fig. 12 Time histories of the acceleration at the top of the solar tower with and without TMD at the critical wind velocity

is 3~16 m/s, corresponding to 11.3~60.1 m/s at the height of 10 m in the prototype (U_{10}). A High Frequency Force Balance (HFFB) is installed at the bottom of the test model to measure the wind-induced base shears and moments, and two accelerometers are installed at the top of the test model to measure the accelerations in the along-wind and cross-wind directions.

The structural damping ratio of the test model of the solar tower was achieved within the range from 0.3% to 2.0% in Li *et al*. (2018). In the present study, the structural damping ratio of the test model is adjusted to be 0.7%, which is close to the prototype value of this kind of solar tower. The time histories of the free vibration acceleration at the top of the test model without and with the tiny TMD are plotted in Figs. 8(a) and (b), respectively. It could be found from Fig. 8 that the decay of the response of the test model with the tiny TMD is obviously faster than that without the tiny TMD. This indicates that the equivalent structural damping ratio of the test model with the tiny TMD is far higher than that without the tiny TMD. The identified structural damping ratio of the test model with the tiny TMD is about 3.6%. Moreover, the test model with tiny TMD is a 2 degree-of-freedom (2-DOF) system, and two neighboring frequency components can be clearly observed in the PSD of the top free vibration acceleration response as shown in Fig. 9.

5. Results of wind tunnel tests

Fig. 10 presents the cross-wind RMS responses of the solar tower with the TMD at the top, together with those without the TMD obtained by Li *et al*. (2018). The wind induced across-wind responses include Root Mean Square (RMS) value of the accelerations at the top (Fig. 10(a)), RMS values of the base shear and the base moment at the bottom (Figs. 10(b) and (c), respectively). It should be noted that these responses have been transferred from the test model to the prototype. Here U_{10} is the prototype mean wind velocity at the height of 10 m. It could be clearly found from Fig. 10 that the across-wind RMS responses of the solar tower are obviously reduced by installing a TMD system at the top, especially for the vortex-induced responses near the critical wind velocity (U_{10} = 23.2 m/s). For example, the RMS value of the across-wind acceleration at the top near the critical wind velocity decreases from 0.263 g (g is the acceleration of gravity) to

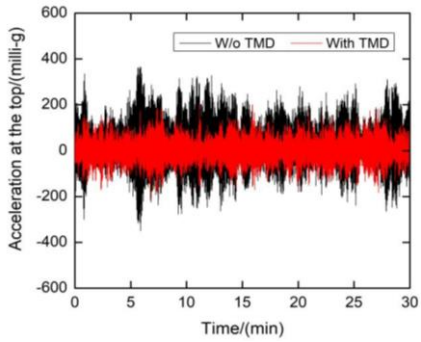

(a) Cross-wind

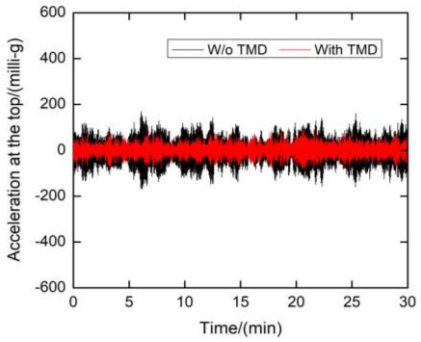

(b) Along-wind

Fig. 13 Time histories of the acceleration at the top of the solar tower with and without TMD at the design wind velocity

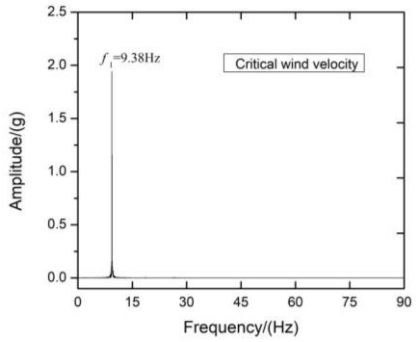

(a) Critical wind velocity

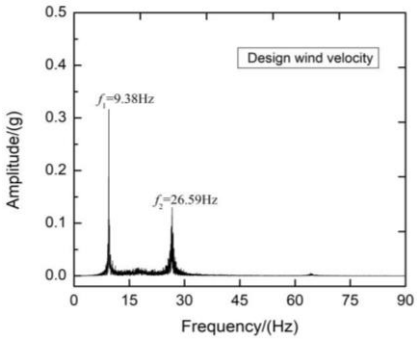

(b) Design wind velocity

Fig. 14 Power spectrum densities of the acceleration at the top without the TMD

0.037 *g*. In the meanwhile, the RMS values of the across-wind base shear and moment at the bottom near the critical wind velocity decrease from 20.6 × 10^3 kN and 29.5 × 10^5 kN·m to 2.83 × 10^3 kN and 3.95 × 10^5 kN·m, respectively, i.e., the RMS responses in the across-wind direction at the critical wind velocity could be reduced about 86% by the TMD system. In addition, it is interesting to find that the critical wind velocity for the solar tower with the TMD, 24.5 m/s, is a little bit larger than that without the TMD, 23.2 m/s. However, the reduction of the across-wind RMS responses at the design wind velocity (U_{10} = 41.0 m/s) is far less than that at the critical wind velocity. For instance, the across-wind RMS values of the acceleration at the top, the base shear and moment at the bottom at the design wind velocity decrease from 0.080*g*, 4.386 × 10^3 kN and 6.09 × 10^5 kN·m to 0.043 *g*, 2.555 × 10^3 kN and 3.47 × 10^5 kN·m, respectively. The RMS responses in the across-wind direction at the design wind velocity could be reduced about 45% by the TMD system.

Fig. 11 presents the along-wind responses of the solar tower with the TMD at the top, together with those without the TMD obtained by Li *et al*. (2018). The wind induced along-wind responses include RMS value of the acceleration at the top (Fig. 11(a)), RMS and mean values of the base shear and the base moment at the bottom (Figs. 11(b) and (c), respectively). It could be found from Fig. 11 that the RMS values of the along-wind responses of the solar tower with the TMD are obviously smaller than those without the TMD. The along-wind RMS values of the acceleration at the top, the base shear and moment at the bottom at the design wind velocity decrease from 0.042 *g*, 2.86 × 10^3 kN and 4.30 × 10^5 kN·m to 0.022*g*, 1.40 × 10^3 kN and 2.02 × 10^5 kN·m, respectively. The RMS responses in the along-wind direction at the design wind velocity could be reduced about 50% by the TMD system. However, it appears that the mean values of the along-wind responses of the solar tower could not be reduced by the TMD, similar to the results obtained in numerical simulation as shown in the work by Lu *et al*. (2017).

Fig. 12 presents the time histories of the accelerations at the top of the solar tower with and without the TMD at the critical wind velocity. It could be found from Fig. 12 the across-wind and along-wind responses of the solar tower at the critical wind velocity could be both obviously reduced, just as the results shown in Figs. 10 and 11. However, the time histories of the accelerations at the top of the solar tower at the design wind velocity, as shown in Fig. 13, indicates that the reduction of the wind-induced responses at the design wind velocity is obviously less than those at the critical wind velocity. Fig. 14 shows the Power Spectrum Density (PSD) of the time histories of the cross-wind acceleration at the top of the solar tower without the TMD. It could be found from Fig. 14 that only one frequency peak (9.38 Hz), which is corresponding to the first natural frequency of the test model, is observed in the PSD of the acceleration at the critical wind velocity, as shown in Fig. 14(a). However, there two frequency peaks (9.38 Hz and 26.59 Hz), corresponding to the first and second natural frequencies of the test model, are found in the PSD of the acceleration at the design wind velocity, as shown in Fig. 14(b). In the present study, the tiny TMD is specially designed to mitigate the oscillation of the first mode. This is the main reason for the obvious difference

Table 2 Comparisons of the peak responses of the solar tower

Types		Critical wind velocity			Design wind velocity		
		Acc.* (g)	Shear (kN)	Moment (kN·m)	Acc.* (g)	Shear (kN)	Moment (kN·m)
Across-wind	W/o TMD	0.352	3.8×10^4	5.96×10^6	0.343	1.91×10^4	3.0×10^6
	With TMD	0.124	1.02×10^4	1.56×10^6	0.203	1.06×10^4	1.61×10^6
	Reduction	65%	73%	74%	41%	45%	46%
Along-wind	W/o TMD	0.179	1.89×10^4	2.85×10^6	0.159	1.81×10^4	2.45×10^6
	With TMD	0.028	0.48×10^4	0.69×10^6	0.087	1.35×10^4	1.95×10^6
	Reduction	84%	75%	76%	45%	25%	20%

* Acc.: Acceleration

between the reductions by the TMD system at the critical and design wind velocities.

The peak across-wind and along-wind responses of the solar tower with and without the TMD system at the critical and design wind velocities (respectively 23.2 m/s and 41.0 m/s), which are the important parameters for the design of this kind of structures, are listed in Table 2. It could be found from Table 2 that the reduction of the peak responses of the solar tower at the critical wind velocity is about 75%, both in the across-wind and along-wind directions. However, the maximum reduction of the responses at the design wind velocity is about 45%, obviously less than that at the critical wind velocity. It seems that the across-wind peak responses are larger than the along-wind responses when the TMD system is not installed on the solar tower (0.7% of damping ratio). However, the along-wind peak responses are larger than the across-wind responses if the TMD system is installed on the solar tower.

6. Conclusions

On the model test, it is difficult to conveniently adjust the parameters of the TMD because of the small size. In this paper, a tiny TMD system by adopting the eddy current technology is specially designed and manufactured for an elastic test model of a 243-meter-high solar tower with a length scale of 1/200. The mass ratio of the TMD system is 1%, and the mass of the tiny TMD for the test model is about 5×10^{-3} kg. A series of numerical simulation by using the COMSOL software is conducted to investigate the effects of three key parameters on the damping coefficient of the tiny eddy current damper. The results of the numerical simulations indicate that the thicknesses of the back iron plate and the conductive plate should be respectively 1 mm and 6 mm in order to realize a target structural damping ratio of 6%. Based on this parameter, a tiny eddy current damper is manufactured to identify its structural damping and determine the distance between the magnet and the conductive plate. The experimental results show that the distance between the magnet and the conductive plate should be 2.5 mm to realize a structural damping ratio of 6% for the tiny TMD. The tiny TMD is installed on the top of the elastic test model, and a series of wind tunnel tests are conducted to investigate the effectiveness of the proposed TMD on suppressing the wind-induced responses of the solar tower. The results show that the wind-induced responses of the solar tower could be effectively mitigated by the installation of the TMD, especially for the cross-wind vortex-induced responses at the critical wind velocity. The cross-wind RMS responses at the critical wind velocity, including the acceleration at the top, base moment and base shear, could be reduced by about 86%. The reduction of the peak responses of the solar tower at the critical wind velocity is about 75%, and the maximum reduction of the responses at the design wind velocity is about 45%, obviously less than that at the critical wind velocity. However, it appears that the mean values of the along-wind responses of the solar tower could not be reduced by the TMD.

Data availability

All data, models, and code generated or used during the study appear in the submitted article.

Acknowledgments

This project is supported by the National Key Research and Development Program of China (Grant No. 2017YFC0703600 and No. 2017YFC0703604).

References

Bae, J.S., Kwak, M.K. and Inman, D.J. (2005), "Vibration suppression of cantilever beam using eddy current damper", *J. Sound Vib*., **284**(3-5), 805-824. https://doi.org/10.1016/j.jsv.2004.07.031.

Bandi, E.K., Tamura, Y., Yoshida, A., Kim, Y.C. and Yang, Q.S. (2013), "Experimental investigation on aerodynamic characteristics of various triangular-section high-rise buildings", *J. Wind Eng. Ind. Aerodyn*., **122**, 60-68. https://doi.org/10.1016/j.jweia.2013.07.002.

Brownjohn, J.M.W., Carden, E.P., Goddard, C.R. and Oudin, G. (2010), "Real-time performance monitoring of tuned mass damper system for a 183 m reinforced concrete chimney", *J.*

Wind Eng. Ind. Aerodyn., **98**, 169-179. https://doi.org/10.1016/j.jweia.2009.10.013.
CICIND (1999), *Model Code for Steel Chimneys*: *Revistion 1 - 1999*, Hemel Hempstead, London, UK.
Cunningham, R.E. (1986), Passive eddy-current damping as a means of vibration control in cryogenic turbomachinery, NASA-TP-2562, NASA, USA.
Den Hartog, J.P. (1956), *Mechanical Vibrations*, McGraw-Hill, New York, USA.
Duan, Y.Y., Wang, W.X., Zhang, P., Huo, L.S. and Song, G. (2020), "New type of pounding tuned mass damper for confined space", *J. Aerosp. Eng*., **33**(4), 04019053. https://doi.org/10.1061/(ASCE)AS.1943-5525.0001138.
Ebrahimi, B., Khamesee, M.B. and Golnaraghi, F. (2009), "Eddy current damper feasibility in automobile suspension: Modeling, simulation and testing", *Smart Mater. Struct*., **18**(1), 015017. https://doi.org/10.1088/0964-1726/18/1/015017.
Facioni, R.J., Kwok, K.C.S. and Samali, B. (1993), "Wind tunnel investigation of active vibration control of tall buildings", *Proceedings of the 3rd Asia-Pacific Symposium on Wind Engineering*, Hong Kong, December.
González-Roubaud, E., Pérez-Osorio, D. and Prieto, C. (2017), "Review of commercial thermal benergy storage in concentrated solar power plants: Steam vs. molten salts", *Renew. Sustain. Energy Rev*., **80**, 133-148. https://doi.org/10.1016/j.rser.2017.05.084.
Gunter, E.J., Humphris, R.R. and Severson, S.J. (1983), Design study of magnetic eddy-current vibration suppression dampers for application to cryogenic turbomachinery, NASA-CR-173273, University of Virginia, USA.
Huang, Z.W., Hua, X.G., Chen, Z.Q. and Niu, H.W. (2018), "Modeling, testing, and validation of an eddy current damper for structural vibration control", *J. Aerosp. Eng*., **31**(5), 04018063. https://doi.org/10.1061/(ASCE)AS.1943-5525.0000891.
Isyumov, N., Dutton, R. and Davenport, A.G. (1989), "Aerodynamic methods for mitigating wind-induced building motions, structural design, analysis and testing", *Proceedings of the Structure Congress '89*, ASCE, New York, USA, August.
Kawamura, M., Maebayashi, K. and Shimada, K. (1993), "Application of a tuned mass damper system using laminated rubber bearing to a tower structure (Design, test and recorded vibration during typhoons)", *Proceedings of International Conference on Tall Buildings*, Rio de Janeiro, Brazil, October.
Kienholz, D.A., Pendleton, S.C. and Richards Jr, K.E. (1994), "Demonstration of solar array vibration suppression", *Proceedings of the North American Conference on Smart Structures and Materials*, Orlando, USA, June.
Kim, Y.C., Tamura, Y., Tanaka, H., Ohtake, K., Bandi, E.K. and Yoshida, A. (2014), "Wind-induced responses of super-tall buildings with various atypical building shapes", *J. Wind Eng. Ind. Aerodyn*., **133**, 191-199. https://doi.org/10.1016/j.jweia.2014.06.004.
Kim, Y.C., Bandi, E.K., Yoshida, A. and Tamura, Y. (2015), "Response characteristics of super-tall buildings – effects of number of sides and helical angle", *J. Wind Eng. Ind. Aerodyn*., **145**, 252-262. https://doi.org/10.1016/j.jweia.2015.07.001.
Kitamura, K., Ohkuma, T., Kanda, J., Mataki, Y. and Kawahata, S. (1988), "Chiba port tower: Full-scale measurement of wind actions (part 1) organisation, measurement system and strong wind data", *J. Wind Eng*., **37**, 401-410. https://doi.org/10.1016/0167-6105(92)90661-S.
Koshimura, K., Tatsumi, M. and Hata, K. (1994), "Vibration control of the main towers of the Akashi Kaikyo Bridge", *Proceedings of the 1st Int. Conference on Structure Control*, Pasadena, USA, August.
Kwak, M.K., Lee, M.I. and Heo, S. (2003), "Vibration suppression using eddy current damper", *Korean Soc. Noise Vib. Eng*., **233**,136-141.
Kwok, K.C.S. (1983), "Full-scale measurements of wind-induced response of Sydney tower", *J. Wind Eng. Ind. Aerodyn*., **14**, 307-318. https://doi.org/10.1016/0167-6105(83)90033-8.
Larose, G.L., Larsen, A. and Svensson, E. (1995), "Modelling of tuned mass dampers for wind-tunnel tests on a full-bridge aeroelastic model", *J. Wind Eng. Ind. Aerodyn*., **54**, 427-437. https://doi.org/10.1016/0167-6105(94)00058-L.
Li, S.Y., Liu, M., Li, H.X., Hui, Y. and Chen, Z.Q. (2018), "Effects of structural damping on wind-induced responses of a 243-meter-high solar tower based on a novel elastic test model", *J. Wind Eng. Ind. Aerodyn*., **172**, 1-11. https://doi.org/10.1016/j.jweia.2017.10.027.
Liu, M., Li, S.Y., Li, H.X., Li, S.K. and Chen, Z.Q. (2019), "Reynolds number effects on the wind-induced responses of a 243-meter-high solar tower in elastic wind tunnel tests", *ASCE J. Aerosp. Eng*., **32**(4), 04019053. https://doi.org/10.1061/(ASCE)AS.1943-5525.0001033.
Lou, W.J., Wen, Z.P., Chen, Y. and Huang, M.F. (2019), "Wind tunnel study on bidirectional vibration control of lattice towers with omnidirectional cantilever-type eddy current TMD", *Appl. Sci*., **9**(15), 2978. https://doi.org/10.3390/app9152978.
Lu, X.L. and Chen, J.R. (2011), "Mitigation of wind-induced responses of Shanghai center tower by tuned mass damper", *Struct. Des. Tall Spec. Build*., **20(**4), 435-452. https://doi.org/10.1002/tal.659.
Lu, X., Zhang, Q., Weng, D., Zhou, Z., Wang, S., Mahin, S.A., Ding, S. and Qian, F. (2017), "Improving performance of a super tall building using a new eddy-current tuned mass damper", *Struct. Control Health Monit.*, **24**(3), e1882. https://doi.org/10.1002/stc.1882.
Mariantonieta, G.S. and Hojjat, A. (2013), "Tuned mass dampers", *Arch. Comput. Methods Eng*., **20**, 419-431. https://doi.org/10.1007/s1183-013-9091-7.
Mcnamara, R.J. and Taylor, D.P. (2003), "Fluid viscous dampers for high-rise buildings", *Struct. Des. Tall Spec. Build*., **12**(2), 145-154. https://doi.org/10.1002/tal.218.
Narkhede, D.I. and Sinha, R. (2014), "Behavior of nonlinear fluid viscous dampers for control of shock vibration", *J. Sound Vib*., **333**(1), 80-98. https://doi.org/10.1016/j.jsv.2013.08.041.
Ohtake, K., Mataki, Y., Nagase, T. and Hisakotu, T. (1992), "Full-scale measurement of wind actions on super high-rise office building in Osaka", *Summ. Tech. Papers Ann. Meeting Arch. Inst. Japan*, **2009**, 17-18.
Quan, Y. and Gu, M. (2005), "Experimental evaluation of aerodynamic damping of square super high-rise buildings", *Wind Struct., Int. J*., **8**(5), 309-324. https://doi.org/10.12989/was.2005.8.5.309.
Sacks, M.P. and Swallow, J.C. (1993), "Tuned mass dampers for towers and buildings", *Proceedings of the Symposium on Structural Engineering in Natural Hazards Mitigation*, Irvine, California, USA, April.
Sakamoto, H., Araki, K., Ishida, A., Kobayashi, S. and Kuwahara, T. (1997), "Design of permanent magnet type compact ECB retarder", SAE Technical Paper 973228, Warrendale, USA.
Tahri, M., Hakdaoui, M. and Maanan, M. (2015), "The evaluation of solar farm locations applying geographic information system and multi-criteria decision-making methods: Case study in southern Morocco", **51**, 1354-1362. https://doi.org/10.1016/j.rser.2015.07.054.
Tamura, Y., Xu, X.D., Tanaka, H., Kim, Y.C., Yoshida, A. and Yang, Q.S. (2017), "Aerodynamic and pedestrian-level wind characteristics of super-tall buildings with various configurations", *Procedia Eng*., **199**, 28-37. https://doi.org/10.1016/j.proeng.2017.09.146.
Tanaka, H. and Mak, C.Y. (1983), "Effect of tuned mass dampers

on wind induced response of tall buildings", *J. Wind Eng. Ind. Aerodyn.*, **14**(1-3), 357-368. https://doi.org/10.1016/0167-6105(83)90037-5.

Tanaka, H., Tamura, T., Ohtake, K., Nakai, M. and Kim, Y.C. (2012), "Experimental investigation of aerodynamic forces and wind pressures acting on tall buildings with various unconventional configurations", *J. Wind Eng. Ind. Aerodyn.*, **107-108**, 179-191. https://doi.org/10.1016/j.jweia.2012.04.014.

Tuan, A.Y. and Shang, G.Q. (2014), "Vibration control in a 101-storey building using a tuned mass damper", *J. Appl. Sci. Eng.*, **17**(2), 141-156. https://doi.org/10.6180/jase.2014.17.205.

Vickery, B.J. and Davenport, A.G. (1971), "An investigation of the behaviour in wind of the proposed Centrepoint tower, in Sydney, Australia", Engineering Science Report BLWT-1-70, University of Western Ontario, Canada.

Wang, W.X., Hua, X.G., Wang, X.Y., Chen, Z.Q. and Song, G. (2018a), "Numerical modeling and experimental study on a novel pounding tuned mass damper", *J. Vib. Control*, **24**(17), 4023-4036. https://doi.org/10.1177/1077546317718714.

Wang, W.X., Hua, X.G., Wang, X.Y., Chen, Z.Q. and Song, G. (2018b), "Mechanical behavior of magnetorheological dampers after long-term operation in a cable vibration control system", *Struct. Control Health Monit.*, **26**(1), e2280. https://doi.org/10.1002/stc.2280.

Wen, Q., Hua, X.G., Chen, Z.Q., Yang, Y. and Niu, H.W. (2016), "Control of human-induced vibrations of a curved cable-stayed bridge: design, implementation, and field validation", *J. Bridge Eng.*, **21**(7), 04016028. https://doi.org/10.1061/(ASCE)BE.1943-5592.0000887.

Xu, H.B., Zhang, C.W., Li, H., Tan, P., Ou, J.P. and Zhou, F.L. (2014), "Active mass driver control system for suppressing wind-induced vibration of the Canton Tower", *Smart Struct. Syst., Int. J.*, **13**(2), 281-303. https://doi.org/10.12989/sss.2014.13.2.281.

Zdravkovich, M.M. (1981), "Review and classification of various aerodynamic and hydrodynamic means for suppressing vortex shedding", *J. Wind Eng. Ind. Aerodyn.*, **7**(2), 145-189. https://doi.org/10.1016/0167-6105(81)90036-2.

BS